Full Potential Solutions of Three-Dimensional Supersonic Flows

Kenneth M. Jones* and Noel A. Talcott Jr.*
NASA Langley Research Center, Hampton, Virginia
and
Vijaya Shankar†
Rockwell International Science Center, Thousand Oaks, California

A nonlinear aerodynamic analysis technique based on the full potential equation in conservative form has been enhanced to allow analysis of more complex geometric configurations. Solution procedures for the equations do not require any specific form of geometry or physical grid system. This results in the capability to analyze very complex geometries easily, provided the posed problem lies within the isentropic restrictions of the full potential theory. To treat embedded subsonic flow, characteristic signal propagation theory is used to monitor the type-dependent flow and a conservative switching scheme is employed to transition from the supersonic marching algorithm to a subsonic relaxation procedure and vice versa. An implicit approximate factorization scheme is used to solve the finite difference equations. These modifications now permit analysis of fully three-dimensional flowfields including the interference effects due to lifting surface wakes. Results are presented showing very good correlations with experimental surface pressure data and aerodynamic force data at both design and off-design operating points. Configurations examined include several waverider concepts, an arrow wing-body with wake, and a fighter forebody-canard configuration.

Introduction

THE most commonly used aerodynamic prediction techniques for the analysis of supersonic flow over three-dimensional surfaces can be classified into two basic categories. Methods based on supersonic linear theory panel methods are applicable to slender configurations at low to moderate supersonic Mach numbers. These methods are restricted by assumptions of isentropic flow, small disturbances, and potential flow, and have limited use for analysis at high angle of attack and/or high supersonic Mach numbers. The second category includes the high supersonic and hypersonic panel methods which use tangent cone, tangent wedge, or similar analysis methods. However, these panel methods are themselves limited in their usefulness because they do not account for interference between surfaces. Despite their inherent restrictions, both categories have successfully analyzed complex three-dimensional geometries with minimum computer time and cost. More sophisticated nonlinear analysis methods based on the solution of the Euler or Navier-Stokes equations exist, but their use as practical prediction techniques for aircraft design is not yet a reality. These techniques also often require an increased level of effort by the user to perform an analysis of even elementary configurations. Thus, there exists a need for a nonlinear supersonic technique that will produce accurate results for complex geometries while making efficient use of computational resources as well as minimizing the required level of user sophistication.

The development of efficient full potential solvers now permits accurate nonlinear aerodynamic analysis of supersonic flow over fairly complex aircraft geometries. These full potential solvers have matured to a point where, in many cases, they are competitive with the more complex Euler and Navier-Stokes solvers without requiring an enormous level of sophistication by the user. It is appropriate to note that the user of a full potential method should be aware of the isentropic limitations of the theory that may restrict its use. In general, though, the theory is expected to perform well as long as the local product of Mach number M and flow deflection angle δ is less than 1 ($M\delta \leq 1$). Another criterion used as a rule of thumb is that the Mach number normal to the shocks should be less than about 1.4. The full potential methods have shown very good agreement with experimental data at low to moderate supersonic Mach numbers and have demonstrated the capability to predict flow characteristics for high supersonic Mach number flows.[1-5] Success has been achieved in predicting surface pressure distributions on various configurations ranging from simple bodies of revolution to a nonconical fighter model having embedded subsonic regions.[1,4,5] The accurate computation of the nonlinear effects in supersonic flows is required to predict the detailed pressure distributions adequately over aircraft surfaces and to provide direction to the researcher when making modifications to the configuration geometry.

This paper is presented in two sections. The first discusses several new modifications to the full potential analysis method of Ref. 1 and the second part will investigate the application of the improved method for the analysis of several complex configurations. These applications include: the conclusion of a study of several waverider concepts, the improved analysis of a previously reported arrow wing-body configuration with wake interference, and the gridding and analysis of a fighter forebody-canard configuration.

Full Potential Analysis Method—Background

The technique of Ref. 2 is based on the full potential equations written in conservative form which conserves mass across shock waves as well as throughout the flow. The

Presented as Paper 84-0139 at the AIAA 22nd Aerospace Sciences Meetings, Reno, NV, Jan. 9-12, 1984; received Oct. 11, 1984; revision received June 19, 1985. This paper is declared a work of the U.S. Government and therefore is in the public domain.

*Aerospace Engineer, High-Speed Aerodynamics Division. Member AIAA.

†Manager, Computational Fluid Dynamics Group. Associate Fellow AIAA.

technique also employs characteristic signal propagation theory to correctly control density biasing for treatment of shocks (including embedded shocks). Reference 1 describes modifications to the method that, in conjunction with the characteristic signal propagation technique, permit treatment of supersonic flows with embedded subsonic regions. Typically these embedded subsonic regions occur near the fuselage-canopy juncture and/or on the leading edge of a moderately swept wing at low supersonic Mach numbers. A conservative switching scheme is employed to transition from the supersonic marching algorithm to a subsonic relaxation procedure and vice versa. An implicit factorization scheme is used to solve the finite differenced equations.

Solution procedures for the equations do not require any specific form of geometry or physical grid system. This results in the capability to analyze very complex geometries easily, provided the problem lies within the isentropic restrictions of the full potential theory. The body-fitted grid system is generated using numerical mapping techniques prior to the solution of the equations. Separation of the gridding and flowfield analysis allows verification of the grid system (distribution, clustering, etc.) before proceeding with the solution. This has proven invaluable in detecting and correcting potential grid problems that would have caused the solution procedure to fail or would have prevented an accurate analysis.

This method is still in the developmental and validation stages. Over the past year considerable progress has been achieved in the complexity of the geometries analyzed, the accuracy of the results obtained, the reduction of execution time, and the ease of the geometry input process. Initially the code was used to successfully analyze simple cones and bodies of revolution at angle of attack.[3] Recent improvements now allow grid generation for complex geometries that can be analyzed with relative ease.[1,4,5] For conical geometries, the grid arrangement is identical in each marching plane and the conical flowfield is assumed to have converged once the rms of the change in density in the marching plane is reduced below a user-specified criterion (typically 10^{-5}). For nonconical geometries, the computational grid must be generated at each marching plane since the configuration no longer has identical cross-sectional shapes. An initial data plane is established near the nose of the configuration by assuming a conical nose shape. Nonconical marching follows and at each nonconical marching plane the density is iterated to convergence before proceeding to the next plane.

The underlying philosophy in developing the method strives for ease of implementation while producing useful output for those working on current aerodynamic problems (e.g., surface pressure distributions and aerodynamic force coefficients). Steps have been taken throughout the code development process to ensure the generality of the input necessary to execute the method. This led to the separation of the equation solution procedure and the gridding process. The code can be executed without a detailed knowledge of the actual solution procedure; all that is required for input is the geometric definition of the configuration and initial flow conditions. This definition can be in the form of an analytic expression or can be obtained through the use of any one of a number of geometry-generation techniques [e.g., a computer-aided design (CAD) package].

Improvements have been added to the grid-generation portion of the code to make this a more versatile analysis technique. The need for these modifications arose as a result of the application of the full potential method to nerly complete aircraft configurations. References 1 and 4 contain the details of these improvements which control the grid density, clustering, and distribution.

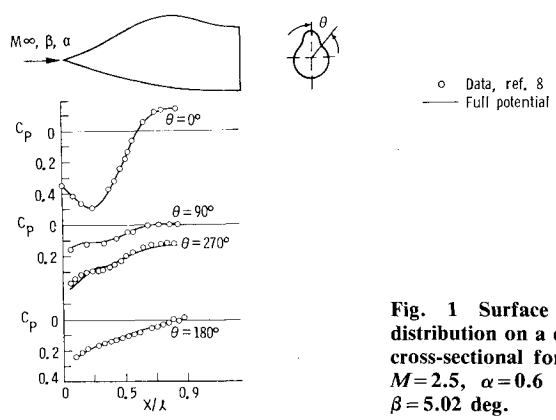

Fig. 1 Surface pressure distribution on a developed cross-sectional forebody at $M=2.5$, $\alpha=0.6$ deg, and $\beta=5.02$ deg.

Enhancements in Method

The application of the full potential method to complex geometries and complete aircraft configurations identified several additional areas in the method where modifications and/or enhancements were required. A short discussion of the additional modifications follows, along with comparisons of analytic results, and experimental data to validate the enhancements.

Angle of Attack and Sideslip Treatment

The complete analysis of an aircraft configuration must address the vehicle's performance under angle of attack α and sideslip β flight conditions. For asymmetric configurations a similar problem exists in that the flowfield is not symmetric and, therefore, requires a solution of the entire cross-flow plane. References 6 and 7 report the details of the addition of sideslip to the full potential code.

Validation of the sideslip modification is demonstrated in Fig. 1, which shows the pressure distribution on a forebody with analytically defined cross sections based on a parabolic arc with a 20-deg half-angle at the nose for $M_\infty=2.5$ and $\beta=5$ deg. The axial pressure distributions compare very well with the experimental data from Ref. 8. Figure 2 shows the circumferential pressure distribution for the same forebody at $x/\ell=0.68$ for $M_\infty=1.7$, $\alpha=10$ deg, and $\beta=5$ deg. The comparison with experimental data is very good. These results, in conjunction with the results reported in Ref. 1, extend the use of the full potential method to complex forebody geometries over a wide range of flight conditions.

Swept Trailing-Edge Treatment

Reference 1 reported the development of a wake treatment for the full potential method. This treatment has now been extended for the case of swept trailing edges as reported in Refs. 6 and 7. Figure 3 shows the pressure distribution on the surface of an arrow-wing configuration at a location $x/\ell=0.8$ for $M_\infty=2.96$ and $\alpha=10$ deg. The improvement in the prediction capability achieved using the modified wake treatment is illustrated. The dashed line represents the result from a no-wake calculation reported in Ref. 3 (where a thin flat plate was imposed behind the trailing edge), and the solid line shows the pressure distribution obtained with wake treatment. The improved analysis technique yields predicted pressures on the body that agree very well with the experimental pressures of Ref. 9. Note that this agreement was achieved even though the boundary conditions imposed at the trailing edge are only approximate. The solid-line upper-surface wake pressures are not identical to solid-line lower-wake pressures (see Ref. 1 for complete details on the wake treatment used in these calculations).

Results to date using the full potential method have demonstrated very good correlation with available experimental data—both surface pressures and aerodynamic force data. Modifications to the method have increased the capability of the analysis procedure to provide pitching moment estimates, component interference modeling (wake ef-

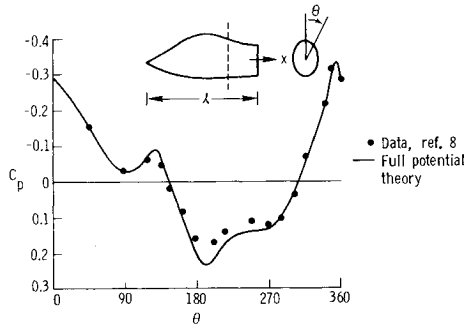

Fig. 2 Circumferential surface pressure distribution at $x/\ell = 0.68$ for $M = 1.7$, $\alpha = 10.0$ deg, and $\beta = 5.02$ deg.

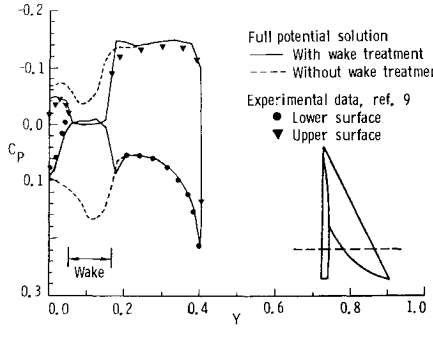

Fig. 3 Arrow-wing surface pressure distribution at $M = 2.96$ and $\alpha = 10.1$ deg.

fects), and full three-dimensional flowfield solutions. The capability now exists to treat configurations with sharp leading and trailing edges, multiple lifting surfaces, and their respective wakes. The results contained in the following sections will demonstrate the use of the improved grid treatment for several complex geometries and will present the first numerical results obtained using these modifications for waverider concepts and the forebody-canard portion of a complex fighter configuration.

Results

Waverider Configurations

Performance requirements for high-speed missiles have led to renewed interest in waverider configurations, particularly waveriders derived from conical shapes.[10,11] Waveriders may meet the missiles requirements for a slender, flat, volumetrically efficient configuration that offers relatively high lift-to-drag ratios (L/D) to achieve the desired range at the required speeds. Typically these vehicles are designed to have a lift-producing lower surface and a low drag, often free-stream aligned, upper surface. Reference 10 emphasizes the fact that a void has existed in techniques capable of analyzing these shapes, particularly at angle of attack and off-design Mach numbers.

In Ref. 4, the full potential method of Ref. 2 was used to investigate several waverider configurations. This paper completes the analysis of configurations based on the elliptic cone waverider shown in Fig. 4. This Mach 4 waverider was derived from flow past an elliptic cone at 0-deg angle of attack.[10] The bottom centerline of this configuration is at an angle of 16.8 deg relative to 0-deg freestream flow. The upper surface is a flat plate with 20 deg anhedral. Reference 4 reported excellent agreement between the calculated surface pressure coefficients and the experimental data over a wide Mach number, angle-of-attack range ($3 \le M \le 5$), (-15 deg $\le \alpha \le 5$ deg). As viscous effects become appreciable or the assumption of isentropic flow is no longer valid, then deviation is observed in the prediction of the data; however, within the limitations of the theory (small flow deflections) the correlation is very good.

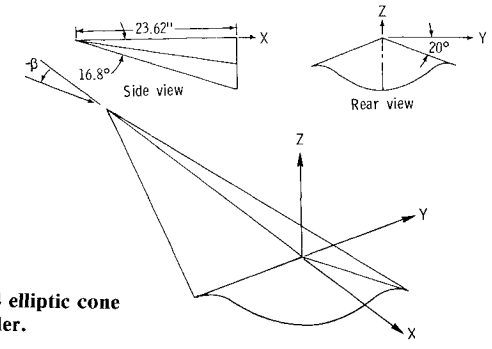

Fig. 4 Mach 4 elliptic cone derived waverider.

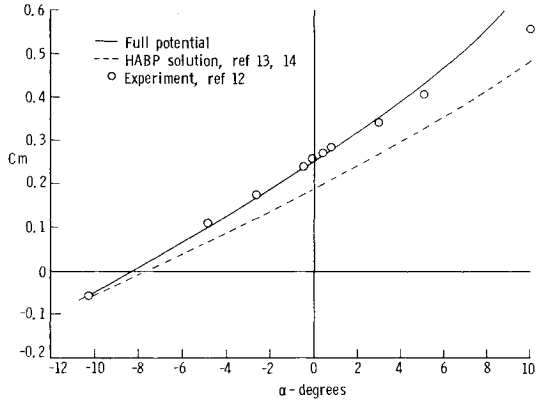

Fig. 5 C_m vs α for an elliptic cone waverider at $M = 4.0$.

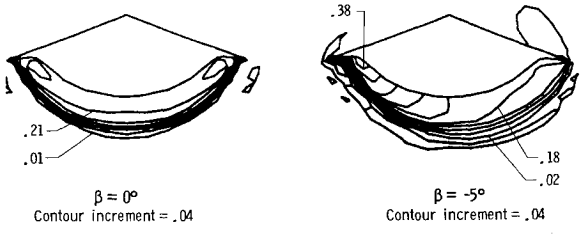

Fig. 6 Pressure coefficient contours for an elliptic cone waverider at $M = 4.0$ and two angles of sideslip.

A pitching moment integration routine and modifications for yaw (three-dimensional flowfield analysis) were used to complete the study of the waverider. Figure 5 presents the comparison for pitching moment vs angle of attack. The correlation is quite good and complements the lift coefficient, C_L, and the drag coefficient, C_D, results presented in Ref. 4. The calculations shown include a Spaulding-Chi (see Ref. 4) viscous correction that was added to the inviscid full potential calculations. The quality of the C_m vs α comparisons provides an indication that the pressure distributions on the configuration are predicted accurately even in areas of the model where there are no experimental data. Pitching moment calculations made using the Hypersonic Arbitrary Body Program (HABP)[13,14] are also included in Fig. 5. The discrepancy between HABP results and experimental data demonstrates the difficulty often experienced when making C_m vs α comparisons using the HABP on configurations where interference effects are significant.

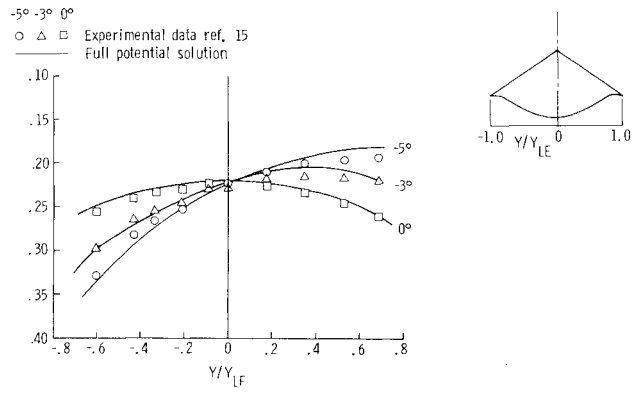

Fig. 7 Elliptic cone waverider lower-surface pressure distribution at $M=4.0$ and various angles of sideslip.

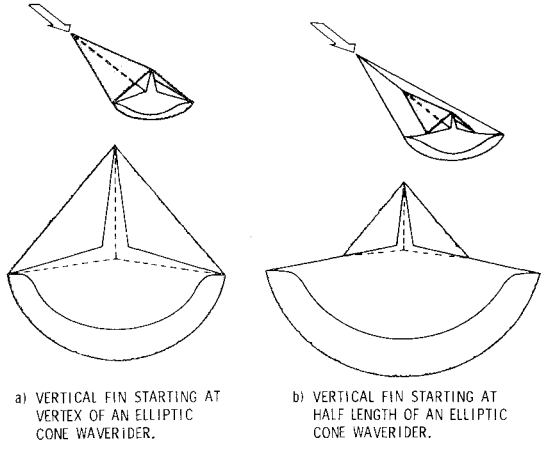

Fig. 8 Elliptic cone waverider with proposed vertical fins.

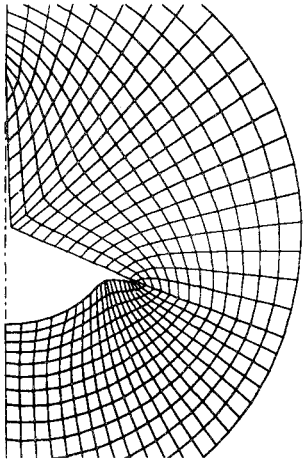

Fig. 9 Computational grid for the waverider with a full-length vertical fin.

The sideslip modification to the full potential method is demonstrated through analysis of the waverider at $M_\infty=4$ and $\alpha=0$ deg for various angles of β. As pointed out previously, the addition of sideslip makes the analysis of the flow fully three-dimensional. In the past, due to symmetry about the vertical centerline, it was only necessary to provide a grid over half of the configuration at various cross-sectional stations along the body. As a result of the addition of sideslip (especially in conjunction with angle of attack), the computational grid must be calculated over the entire circumference at each cross section along the body. The grid remains fixed for all computations (combinations of α and β) at a given freestream Mach number. The grid and location of the outer freestream boundary are often adjusted when the Mach number is changed. For these computations program memory was not increased, therefore, the grid resolution around the configuration was less than that used in the previous analysis (same number of grid points in both cases). A reduction in grid resolution may affect the accuracy of the results depending on the configuration, and program memory (grid array size) may need to be increased.

The full 360-deg computational grid was generated and the waverider was analyzed at Mach 4 for 0-deg angle of attack and various angles of sideslip ranging from -5 to 0 deg. Calculated flowfield pressure coefficient contours for two angles of sideslip ($\beta=0$ and -5 deg) are shown in Fig. 6 at the aft end of the conical waverider. At the design point ($M_\infty=4$, $\alpha=0$ deg, $\beta=0$ deg) the shock is contained by the tips of the waverider and lies below the configuration. The pressure coefficient contour pattern for the off-design point, $\beta=-5$ deg, exhibits the anticipated result that on the windward side of the waverider the shock location has shifted inboard, while on the leeward side the shock has moved off the tip and there is some expansion of the flow around the tip onto the upper surface. The comparison between the calculated results and experimentally obtained surface pressure data[15] for various angles of sideslip is shown in Fig. 7. The correlation between theory and experiment is quite good over the angle-of-sideslip range shown. Results are not presented beyond the 70% semispan location due to a lack of experimental data in the tip region of the configuration. For larger angles of sideslip, such as $\beta=-10$ deg, the isentropic, inviscid assumptions of full potential theory are violated making accurate computation of results impossible. This is primarily due to the large deflections of the flow along the windward side of the waverider.

Reference 15 discusses in detail the need for and hypothesize the design of control surfaces for the elliptic cone waverider. They suggest that control surfaces, such as flaps and ailerons, can be built into the trailing edges of either the flat upper surfaces or the curved lower surface of the waverider. However, in order to provide adequate lateral control a vertical fin would be required. Two possible fin designs were postulated in Ref. 15 and are reproduced in Fig. 8 (for clarity the fins are shown thicker than they would actually be). One vertical fin begins at the vertex of the waverider, while the other begins at a location half of the total body length behind the nose. Both of the fins are based on caret-waverider designs which produce two-dimensional flow behind planar oblique shock waves. The shock wave below the waverider and the plane shock waves generated by the fins/upper surface are illustrated on Fig. 8. It should be noted that for any of these control surfaces the flowfield will be know exactly at the design point ($M_\infty=4$, $\alpha=0$ deg), therefore, their control performance can be estimated. Again, the off-design characteristics will require the use of a numerical method, such as the full potential method, to estimate performance.

To demonstrate the applicability of the full potential method the waverider configuration with the full length fin of Fig. 8 was analyzed. No experimental data is available for this configuration. The computational grid for the full-length fin waverider is shown in Fig. 9. Again, the vertical fin required to produce the correct planar shock patterns is much thinner than that illustrated in Fig. 8. Even with the very thin vertical fin, no special gridding procedures were required to generate the grid. Figure 10 contains examples of two flowfield pressure coefficient contour plots obtained in the analysis. The plot of the left shows the results obtained at the on-design condition of $M_\infty=4$ and $\alpha=0$ deg. The planar shock pattern predicted by the full potential code is very similar to that shown in Fig. 8 for the full-length fin. It should be noted, however, that there is a significant dif-

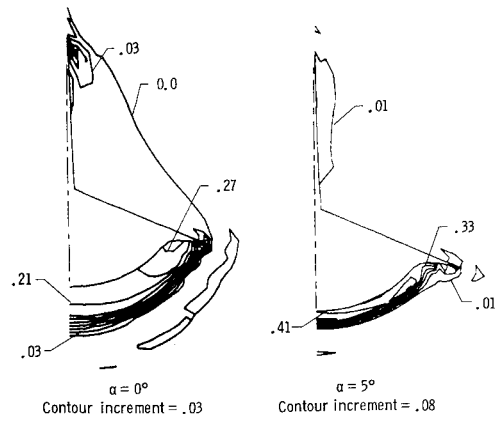

Fig. 10 Pressure coefficient contours for the waverider with a full-length vertical fin at $M=4.0$ and two angles of attack.

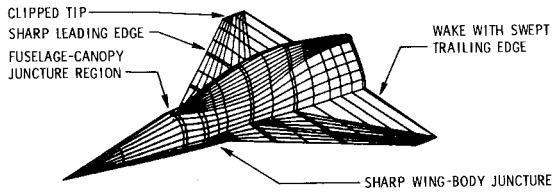

Fig. 11 Potential problem areas in an analysis of a fighter forebody-canard configuration.

ference in shock strength between the shock wave below the waverider and the planar shock.

As stated earlier, the advantage of the full potential method is its ability to analyze these waveriders at off-design conditions to evaluate their performance. The second contour plot of Fig. 10 contains the results obtained at 5-deg angle of attack. As expected, the lower-surface shock moves closer to the surface at the body and matches the analysis of Ref. 4. In the upper-surface flowfield a shock wave is attached to the vertical wedge portion of the fin and there is an expansion field over the horizontal portion of the upper surface of the waverider. Attempts to analyze the waverider-fin combination at -5-deg angle of attack have not been successful. The flow at the tip of this very sharp, thin, vertical fin poses an extremely difficult problem for an inviscid method. In reality, there are probably strong viscous effects occurring at the tip. To accommodate configurations incorporating very thin sharp tips will require further modifications to the method. These are currently under development.

Fighter Forebody-Canard Configuration

The ability to analyze realistic configurations accurately, efficiently, and with relative ease in the goal behind continued development of the full potential code. At the present time the code is not capable of solving the flowfield over a complete, complex fighter configuration, but it can tackle the analysis of the flow over the forward portion of the vehicle. The forebody-canopy-canard portion of a complex fighter configuration is a challenging case because certain problem areas arise that must be addressed prior to the analysis of the configuration. The problem areas are highlighted in Fig. 11. These items are not specific to this particular configuration but are generic ones that could occur on any configuration.

Sharp leading edges present two problems: they are difficult to grid and very difficult to analyze accurately. Flowfields at and/or near a sharp edge are often dominated by viscous effects (e.g., separation, formation of vortices, etc.) which cannot be accounted for by an inviscid code.

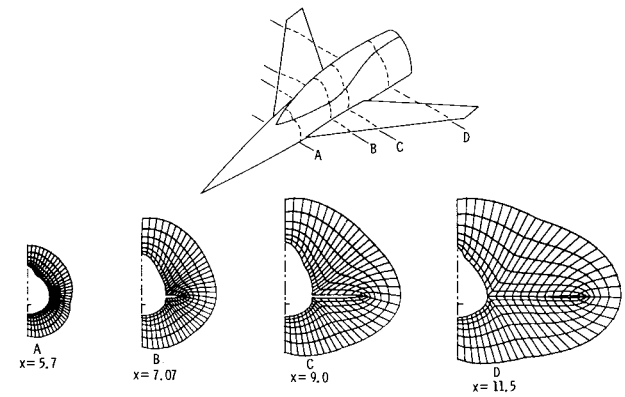

Fig. 12 Fighter forebody-canard configuration with computational grids.

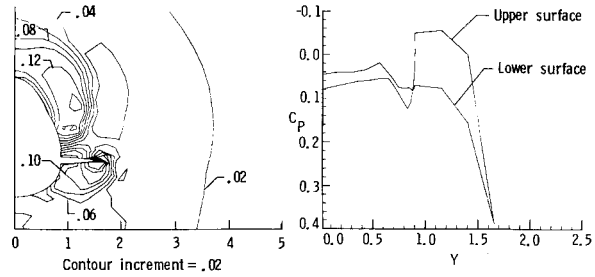

Fig. 13 Pressure coefficient contours and surface pressure distribution on a fighter forebody-canard configuration at $x=7.07$.

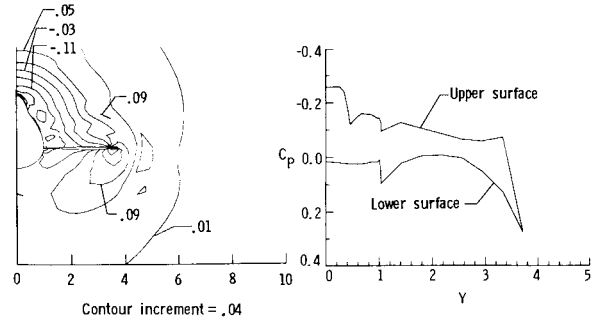

Fig. 14 Pressure coefficient contours and surface pressure distribution on a fighter forebody-canard configuration at $x=10.0$.

Modifications previously made to the method enable the code to solve the flow around the edge, but when viscous effects become appreciable the results will no longer be reliable. The fighter canard has the added complication that the sharp edge suddenly develops out of the smooth forebody shape. This produced a sharp discontinuity that results in the formation of a leading-edge shock at the canard-body juncture. To accommodate the developing wing, it has been observed that small marching step sizes are required in this region.

The clipped tip of the canard (or wing) is another area dominated by viscous effects. A strong vortex will develop at the clipped edge of the canard. To prevent the code from failing at the tip, large marching step sizes are taken to minimize error propagation and a tip treatment is employed.

At the fuselage-canopy juncture, a canopy shock will form and at low supersonic Mach numbers a small embedded subsonic pocket may be present. If subsonic flow is detected, the full potential method automatically switches from the marching algorithm to relaxation procedure. The analysis of this fighter forebody-canopy-canard geometry encountered no subsonic flow.

The wake treatment modification discussed in Ref. 1 accounts for wakes behind trailing edges of lifting surfaces. For this fighter configuration the wake situation is complicated by the swept trailing edge. At cross-sectional stations downstream of the root chord trailing edge, the canard appears to be detached from the body in the computational cross-sectional plane. The wake boundary conditions are applied along a line or wake slit between the body and canard. Once the above-mentioned problem areas are addressed analysis of the forebody-canard configuration is possible.

The first step in the analysis is to generate the computational grid. An isometric view of some of the more significant computational grid stations is shown in Fig. 12. At $x=5.7$, the fuselage and canopy are evident in the cross-sectional shape but the canard has not developed yet. However, points have been clustered on the fuselage near the location where the canard will emerge. These clustered points eventually become the points on the surface of the canard as shown in the grid at $x=7.07$. The grid station at $x=9.0$ is just ahead of the trailing edge of the canard root. At $x=11.5$ the canard and forebody appear as two separate bodies. They are connected by a wake slit on which the wake boundary condition is imposed.

Figures 13-16 are examples of results obtained from the analysis of the fighter configuration at the cruise condition of $M_\infty=2$, $\alpha=4$ deg. In each figure both the surface pressure distribution and the flowfield pressure coefficient contours are displayed. A canopy shock forms at the fuselage-canopy juncture and as the analysis proceeds downstream this shock continues to move outward. This is clear from the calculations presented at $x=7.07$ in Fig. 13.

The pressure field produced by the canopy is felt by the canard as we proceed downstream and is seen in Fig. 14 at an x station of 10.0. These results are just ahead of the canard root trailing edge and we see a typical lifting surface pressure distribution on the canard. At $x=11.0$, Fig. 15, the canard wake slit treatment is now present and the surface pressure distribution provides a good example of the type of results that should occur in this region. Lift is still being produced on the canard, but in the wake region the pressures on the upper and lower surfaces of the wake nearly match. There is little difference in pressure across the wake slit. Other features of the flow that can be pointed out are the shock and expansion occurring on the upper and lower surfaces of the trailing edge of the canard at the wake slit boundary.

At $x=12.5$, Fig. 16, the canard cross-sectional width is very small and barely visible in the pressure contour plot. However, the pressure coefficient contours do show that the canard still causes a disturbance in the flowfield. A plot of the surface pressure distributions again demonstrates the near match of pressure on the upper and lower surfaces of the wake slit. Some lift is still being produced by the small amount of canard at this cross section. Presently, no experimental data is available for comparison with theoretical results but the trends displayed by these results are those that were expected.

To fully compute the flow about a complete supersonic fighter configuration requires the method to address several additional problem areas such as those highlighted in Fig. 17. Many of these problems have already been addressed with the analysis performed to date. However, the engine/nacelle modeling problem and the handling of multiple lifting surfaces and wakes are still being studied. The multiple lifting surface problem will require some extension of the wake treatment already provided. Numerical studies complemented with an experimental program are planned to determine how the wake of one lifting surface affects the flowfield of a downstream lifting surface particularly at the leading edge. Validation of the method to handle multiple lifting surfaces is required to provide accurate estimates of the performance of advanced concepts such as the fighter

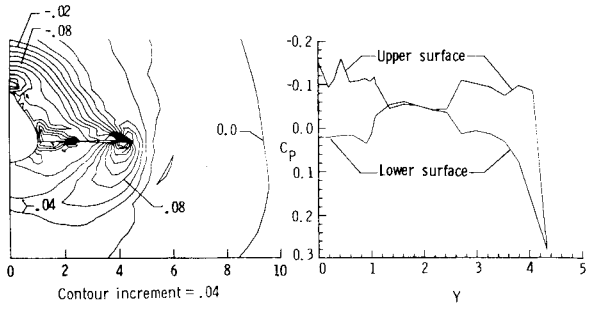

Fig. 15 Pressure coefficient contours and surface pressure distribution on a fighter forebody-canard configuration at $x=11.0$.

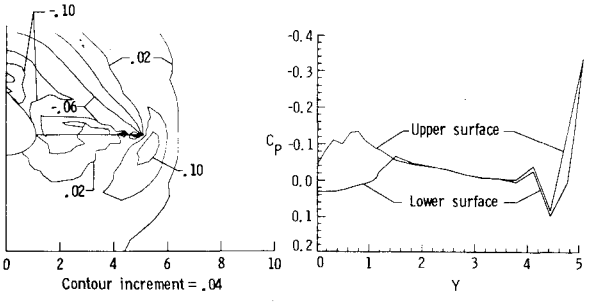

Fig. 16 Pressure coefficient contours and surface pressure distribution on a fighter forebody-canard configuration at $x=12.5$.

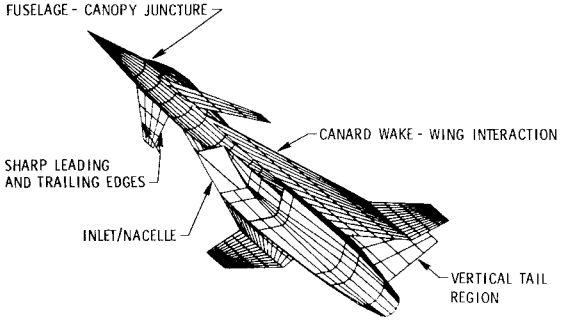

Fig. 17 Problem areas in the analysis of a complex fighter configuration.

configuration shown. The engine/nacelle modeling problem will require more extensive modifications. The internal aerodynamics of the engine will not be analyzed with the full potential method but present plans include capturing the flowfield at the inlet of the engine for correct modeling of the flow around the nacelle. Studies will be made to estimate the best approach to model the exhaust flow at the nozzle, although at present a flowthrough model is planned (flow in equals flow out). Once these modifications are complete, the full potential method will have met its goal to compute the flow about and estimate the performance characteristics of a complex, realistic aircraft configuration.

Conclusions

A nonlinear analysis code based on the conservative full potential equation has been modified and now can be used to examine the inviscid flowfields over many different configurations. Recent modifications are documented herein, including: lifting surface wake treatment, full three-dimensional flowfield solutions, and grid treatment for complex configurations. Comparison of results using the above modifications with experimental data shows that the improved full potential method can be used to analyze complex configurations.

An analysis of several waverider configurations has demonstrated good correlation with experimental data within the limitations of potential theory at both on- and off-design Mach numbers and various angles of attack and for various sideslip angles at 0-deg angle of attack. These correlations include: surface pressure distributions, areodynamic forces (lift, drag, and pitching moment), and flowfield pressure contours.

A modified waverider concept was also analyzed with the modified full potential code. This waverider was derived from the Mach 4 elliptic cone waverider and included an upper-surface vertical fin derived from caret-waverider principles. The analysis of this configuration produced the expected flowfields at both on- and off-design flight conditions.

The versatility of the improved full potential code was demonstrated with the analysis of the forebody-canopy-canard portion of an advanced supersonic fighter concept. Many potential problem areas in the analysis of complex configurations are present in this configuration. Some of these areas were addressed herein and they required some general modifications to the code in conjunction with the major modifications outlined above. Although there are no experimental data available for comparison, the calculations from the full potential code produce the expected trends.

References

[1]Shankar, V., Szema, K., and Osher, S., "Treatment of Supersonic Flows with Embedded Subsonic Regions," *AIAA Journal,* Vol. 23, Jan. 1985, pp. 41-48.

[2]Clever, W. C. and Shankar, V., "Nonlinear Potential Analysis Techniques for Supersonic/Hypersonic Configuration Design," NASA CR-166078, April 1983.

[3]Shankar, V., "Conservative Full Potential Implicit Marching Scheme for Supersonic Flows," *AIAA Journal*, Vol. 20, Nov. 1982, pp. 1508-1514.

[4]Jones, K. M., "Application of a Full Potential Method for Predicting Supersonic Flow Fields and Aerodynamic Characteristics," AIAA Paper 83-1802, July 1983.

[5]Szema, K. Y. and Shankar, V., "Nonlinear Computation of Wing-Body-Vertical Tail-Wake Flows at Low Supersonic Speeds," AIAA Paper 84-0427, Jan. 1984.

[6]Jones, K. M., Talcott, N. A. Jr., and Shankar, V., "Application of a Full Potential Method for Computation of Three-Dimensional Supersonic Flows," AIAA Paper 84-0139, Jan. 1984.

[7]Clever, W. C. and Shankar, V., "Nonlinear Potential Analysis Techniques for Supersonic/Hypersonic Aerodynamic Design," NASA CR-172279, March 1984.

[8]Townsend, J. C., Howell, D. T., Collins, I. K., and Hayes, C., "Surface Pressure Data on a Series of Analytic Forebodies at Mach Numbers from 1.7 to 4.5 and Combined Angles of Attack and Sideslip," NASA TM 80062, June 1979.

[9]Townsend, J. C., "Pressure Data for Four Analytically Defined Arrow Wings in Supersonic Flow," NASA TM 81835, Sept. 1980.

[10]Jischke, M. C., Rasmussen, M. L., and Daniel, D. C., "Experimental Surface Pressures on Cone-Derived Waveriders for $M_\infty = 3.5$," *Journal of Spacecraft and Rockets,* Vol. 20, Nov.-Dec. 1983, pp. 539-545.

[11]Schindel, L. H., "Design of High Performance Hypersonic Missiles," AIAA Paper 82-0391, Jan. 1982.

[12]Rasmussen, M. L., Jischke, M. C., and Daniel, D. C., "Experimental Forces and Moments on Cone-Derived Waveriders for $M_\infty = 3$ to 5," *Journal of Spacecraft and Rockets,* Vol. 19, Nov.-Dec. 1982, pp. 592-598.

[13]Gentry, A. E. and Smythe, D. E., "Hypersonic Arbitrary-Body Aerodynamic Computer Program (Mark III Version), Vol. I—User's Manual," McDonnell Douglas Corp., Long Bearch, CA, Rept. DAC 61552, (available from DTIC as 851811), April 1968.

[14]Gentry, A. E. and Smythe, D. N., "Hypersonic Arbitrary-Body Aerodynamic Computer Program (Mark III Version), Vol II—Program Formulation and Listing," McDonnell Douglas Corp., Rept, DAC 61552, (available from DTIC as 851812), April 1968.

[15]Rasmussen, M. L., "Waverider Configurations Derived from Inclined Circular and Elliptic Cones," *Journal of Spacecraft and Rockets,* Vol. 17, Dec. 1980, pp. 537-545.